

# Accurate Estimation of Scattering Strength Distribution by Simultaneous Reception of Ultrasonic Echoes with Multichannel Transducer Array

Yusaku ABE, Hideyuki HASEGAWA, and Hiroshi KANAI\*

Graduate School of Engineering, Tohoku University, Sendai 980-8579, Japan

(Received November 24, 2006; accepted April 4, 2007; published online July 26, 2007)

Recently, there have been several studies on ultrasonic cross-sectional imaging based on simultaneous reception of echo signals with an array transducer without scanning ultrasonic beams during transmission. In those studies, parallel processing was applied to create an image from a data set simultaneously received by the array. However, the lateral resolution of the parallel processing is not high. In this study, in order to improve the spatial resolution of parallel processing, the least-squares estimation and the truncated singular value decomposition (tSVD) are applied to the echo signals from two wire targets simultaneously received with a multichannel transducer array. We introduced a weighting for correcting the effect of the directivity of the elements of the array. The experimental results show a higher lateral resolution of the tSVD method with weighting than that of conventional parallel processing. The axial resolution is also improved by considering the finite duration of the transmitted ultrasonic pulse. A typical application of this method is nondestructive evaluation, that is, the detection of cavities and cracks in welded metal structures. [DOI: 10.1143/JJAP.46.4813]

KEYWORDS: synthetic aperture, parallel processing, truncated singular value decomposition, simultaneous reception, lateral resolution, frame rate

## 1. Introduction

In some methods reported in literature,<sup>1–5)</sup> echo signals are simultaneously received by all elements of a linear array transducer without forming or scanning ultrasonic beams during transmission. To create an image from a data set simultaneously received by the array, the parallel processing technique<sup>6)</sup> is used. In this method, multiple receiving beams are formed simultaneously within a wide transmitted beam (or spherical wave insonification). This imaging procedure achieves a high frame rate which cannot be realized by conventional B-mode imaging with scanning of thin ultrasonic beams during transmission. Such methods based on simultaneous reception has been applied to flow imaging,<sup>1)</sup> the measurement of two-dimensional motion vectors,<sup>2,3)</sup> and real-time three-dimensional imaging.<sup>4,5)</sup> Furthermore, synthetic aperture processing,<sup>7)</sup> which generates a wide effective aperture by means of several transmissions, can be combined with parallel processing to improve the spatial resolution.

Parallel beam forming (PBF), which is performed by means of time-delay focusing, achieves spatially matched filtering,<sup>5,8)</sup> which maximizes the signal-to-noise ratio (SNR) at each point. However, the lateral resolution of the PBF is lower than that of conventional phased array beam forming because the directivity of the transmitting beam is weak in parallel processing.

Some methods for inverse filtering of simultaneously received echoes have been introduced in order to improve the lateral resolution.<sup>9,10)</sup> These methods are based on the discrete propagation model of ultrasonic pulse echoes and on solving the inverse problem in order to estimate the scattering strength distribution from received signals.<sup>11,12)</sup> However, this inverse problem is difficult to solve under some conditions. In such a situation, small errors in measured data produce large errors in the estimated results.<sup>13)</sup> For the application of these inverse filtering methods, weighting to the receiving aperture should be considered. Because the elements of a transducer array have

directivity, the contributions of the received signals to the estimation are not equal. If the difference in the amplitudes of received signals is not considered in the propagation model, it induces large errors in the estimation.

In this study, to increase the lateral resolution, the scattering strength distribution in the region of interest (ROI) is estimated by applying the least squares (LS) method and truncated singular value decomposition (tSVD) to the simultaneously received echo signals from two wire targets during one transmission. The spatial resolution in the separation of the scatterers is compared with that of PBF, and the effects of weighting and truncation are investigated. A typical application of this method is nondestructive evaluation (NDE), that is, the detection of cavities and cracks in welded metal structures. To investigate other applications, we analyzed the influences of noise on these estimators.

## 2. Principles

### 2.1 Discrete model of pulse echo measurement

To apply inverse filtering, a linear discrete model of pulse echo measurement is employed.<sup>12)</sup> As shown in Fig. 1, the scattering strength distribution in the region of interest (ROI) is discretized in an  $M \times N$  matrix,  $\mathbf{O}$ . The scattering strength at position  $(x_m, z_n)$  ( $m = 0, 1, \dots, M - 1$ ;  $n = 0, 1, \dots, N - 1$ ) is represented by an element  $(\mathbf{O})_{m,n}$  of the matrix. An ultrasonic pulse emitted from a transmitting position,  $x_T$ , is insonified to the entire ROI and is reflected by scatterers in the ROI. The echo is received at positions  $\{x_{R_j}\}$  ( $j = 0, 1, \dots, L - 1$ ) of  $L$  elements simultaneously. The sampled  $K$ -length echo signals,  $\{y_j(k)\}$  ( $k = 0, 1, \dots, K - 1$ ), obtained at receiving position  $x_{R_j}$  are represented by a  $K$ -dimensional vector,  $\mathbf{y}_j = [y_j(0)y_j(1) \cdots y_j(K - 1)]^T$ , where  $T$  denotes a transpose. The amplitudes of the received signals vary depending on the receiving positions because of attenuation, spreading loss, and the directivity of an element. Therefore, in this paper, the weighting function,  $\{w_j^{(m,n)}\}$ , is introduced to show the change in the amplitude of the received signal. Thus, the received signal is expressed as

\*E-mail address: hkanai@ecei.tohoku.ac.jp

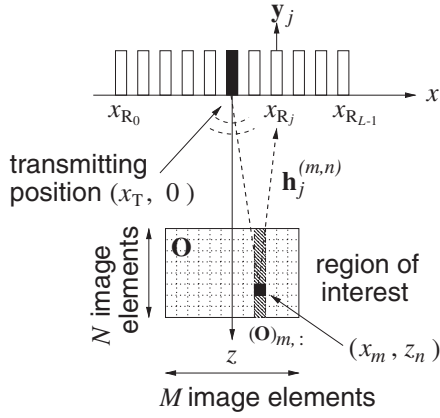


Fig. 1. Schematic view of the ultrasonic measurement system.

$$\mathbf{y}_j = \sum_{m=0}^{M-1} \sum_{n=0}^{N-1} w_j^{(m,n)} \mathbf{h}_j^{(m,n)} (\mathbf{O})_{m,n}, \quad (2.1)$$

where the  $K$ -dimensional vector  $\mathbf{h}_j^{(m,n)}$  shows the discrete impulse response which corresponds to the delay due to propagation from the transmitting point  $(x_T, 0)$  to a receiving point  $(x_{R_j}, 0)$  via point  $(x_m, z_n)$ . The integral ratio of the propagation delay,  $k_j^{(m,n)}$ , to the sampling period,  $T_s$ , is given by

$$k_j^{(m,n)} = \frac{\sqrt{(x_T - x_m)^2 + z_n^2} + \sqrt{(x_m - x_{R_j})^2 + z_n^2}}{cT_s}, \quad (2.2)$$

where  $c$  is the speed of sound in water. The  $K$ -dimensional vector,  $\mathbf{h}_j^{(m,n)}$ , is given by

$$(\mathbf{h}_j^{(m,n)})_k = \begin{cases} 1 & \text{if } k = k_j^{(m,n)} \text{ given by eq. (2.2),} \\ 0 & \text{otherwise.} \end{cases} \quad (2.3)$$

The transmitted ultrasonic pulse is not the impulse, and it has a finite pulse duration. The ultrasonic pulse transmitted from a transducer is expressed by the convolution of the pulse waveform,  $s(k)$ , which is determined by the frequency response of the transducer, and the delayed impulse,  $\mathbf{h}_j^{(m,n)}$ . Therefore, let  $\mathbf{S}$  be a  $K \times K$  lower triangular matrix showing the waveform of the transmitted pulse,  $s(k)$ , such that

$$\mathbf{S} = \begin{pmatrix} s(0) & 0 & 0 & \dots & 0 \\ s(1) & s(0) & 0 & \dots & 0 \\ s(2) & s(1) & s(0) & \ddots & \vdots \\ \vdots & \vdots & \ddots & \ddots & 0 \\ s(K-1) & s(K-2) & \dots & s(1) & s(0) \end{pmatrix}. \quad (2.4)$$

The  $K \times N$  matrix,  $\mathbf{p}_{j,m} = \mathbf{S}[w_j^{(m,0)} \mathbf{h}_j^{(m,0)} \dots w_j^{(m,N-1)} \mathbf{h}_j^{(m,N-1)}]$ , is formed for all combinations of  $j$  and  $m$ . The propagation matrix,  $\mathbf{P}$ , which is a  $KL \times MN$  matrix is constructed as

$$\mathbf{P} = \begin{pmatrix} \mathbf{p}_{0,0} & \mathbf{p}_{0,1} & \dots & \mathbf{p}_{0,M-1} \\ \mathbf{p}_{1,0} & \mathbf{p}_{1,1} & \dots & \mathbf{p}_{1,M-1} \\ \vdots & \vdots & \ddots & \vdots \\ \mathbf{p}_{L-1,0} & \mathbf{p}_{L-1,1} & \dots & \mathbf{p}_{L-1,M-1} \end{pmatrix}. \quad (2.5)$$

The  $L$  vectors  $\mathbf{y}_0, \dots, \mathbf{y}_{L-1}$  are stacked on each other to form a  $KL$ -dimensional vector,  $\mathbf{y} = [\mathbf{y}_0^T \mathbf{y}_1^T \dots \mathbf{y}_{L-1}^T]^T$ . In a similar

way, the  $N$ -dimensional row vectors  $\{(\mathbf{O})_{m,:}\}$  of  $\mathbf{O}$  in Fig. 1 are arranged to form an  $MN$ -dimensional vector,  $\mathbf{o} = [(\mathbf{O})_{0,:} (\mathbf{O})_{1,:} \dots (\mathbf{O})_{M-1,:}]^T$ . Using the propagation matrix  $\mathbf{P}$ , eq. (2.1) is simply rewritten as

$$\mathbf{y} = \mathbf{P}\mathbf{o} + \mathbf{e}, \quad (2.6)$$

where  $\mathbf{e}$  is a  $KL$ -dimensional vector corresponding to additive noise.

### 2.2 Estimation of scattering strength distribution

Let us regard the estimation of the scattering strength distribution as an inverse problem. We follow Lingvall's method<sup>14)</sup> and the inverse filtering is applied as presented below. It is assumed that noise,  $\mathbf{e}$ , is white and has no correlation among the receiving positions  $\{x_{R_j}\}$ . The least-squares solution of eq. (2.6), denoted by  $\hat{\mathbf{o}}_{LS}$ , is given by minimizing the power of noise  $\mathbf{e}$ ,  $J_{LS}$ , as

$$J_{LS} = \|\mathbf{y} - \mathbf{P}\mathbf{o}\|^2 = \mathbf{y}^T \mathbf{y} - 2\mathbf{o}^T \mathbf{P}^T \mathbf{y} + \mathbf{o}^T \mathbf{P}^T \mathbf{P} \mathbf{o}. \quad (2.7)$$

Setting the partial derivative of  $J_{LS}$  with respect to  $\mathbf{o}^T$  to zero, the normal equation is obtained as

$$\mathbf{P}^T \mathbf{P} \mathbf{o} = \mathbf{P}^T \mathbf{y}. \quad (2.8)$$

The solution of eq. (2.8) is given by

$$\hat{\mathbf{o}}_{LS} = (\mathbf{P}^T \mathbf{P})^{-1} \mathbf{P}^T \mathbf{y}. \quad (2.9)$$

In this study, eq. (2.6) is over-determined ( $KL > MN$ ). If matrix  $\mathbf{P}$  is full rank, a unique LS solution exists.

The singular value decomposition (SVD) of matrix  $\mathbf{P}$  is given by

$$\mathbf{P} = \mathbf{U}\mathbf{\Sigma}\mathbf{V}^T, \quad (2.10)$$

where  $\mathbf{U}$  and  $\mathbf{V}$  are  $KL \times KL$  and  $MN \times MN$  orthogonal matrices composed of the eigenvectors of  $\mathbf{P}\mathbf{P}^T$  and  $\mathbf{P}^T\mathbf{P}$ , respectively. Using the SVD, matrices  $\mathbf{U}$  and  $\mathbf{V}$  are determined uniquely.  $\mathbf{\Sigma} = \text{diag}[\sigma_1 \sigma_2 \dots \sigma_{MN}]$  is a  $KL \times MN$  diagonal matrix and  $\sigma_i$  is the  $i$ -th singular value, where  $\sigma_1 \geq \sigma_2 \geq \dots \geq \sigma_{MN}$ . The singular values are the square roots of the eigenvalues of both  $\mathbf{P}\mathbf{P}^T$  and  $\mathbf{P}^T\mathbf{P}$ . In the tSVD, the nonsignificant singular values are set to zero. Using the tSVD, the pseudo-inverse matrix of  $\mathbf{P}$  is given by

$$\mathbf{P}_r^+ = \mathbf{V}\mathbf{\Sigma}_r^+ \mathbf{U}^T, \quad (2.11)$$

where  $\mathbf{\Sigma}_r^+ = \text{diag}[\sigma_1^{-1} \sigma_2^{-1} \dots \sigma_r^{-1} 0 \dots 0]$  is a  $MN \times KL$  diagonal matrix, and  $r$  is the truncation order. By substituting eq. (2.11) into eq. (2.9), the tSVD estimate,  $\hat{\mathbf{o}}_{tSVD}$ , is given by

$$\hat{\mathbf{o}}_{tSVD} = \mathbf{P}_r^+ \mathbf{y}. \quad (2.12)$$

Using the vectors,  $\{\mathbf{h}_j^{(m,n)}\}$ , in eq. (2.3) as a focusing delay, the PBF estimation at point  $(x_m, z_n)$  is given by

$$(\hat{\mathbf{O}}_{\text{PBF}})_{m,n} = \sum_{j=0}^{L-1} (\mathbf{h}_j^{(m,n)})^T \mathbf{y}_j. \quad (2.13)$$

The values  $\hat{\mathbf{O}}_{\text{PBF}}$ ,  $(\mathbf{h}_j^{(m,n)})^T$ , and  $\mathbf{y}_j$  are rearranged in the same way as eq. (2.5), and the PBF estimation is obtained as

$$\hat{\mathbf{O}}_{\text{PBF}} = \mathbf{P}^T \mathbf{y}. \quad (2.14)$$

The PBF estimation is obtained by the product of the transpose of  $\mathbf{P}$  and the received signals  $\mathbf{y}$ . In the PBF, the waveform of the transmit pulse  $s(k)$  is not considered ( $\mathbf{S} = \mathbf{I}$ ,

**I**: identity matrix) in propagation matrix **P** in eq. (2.14) in order to perform only the coherent summation of the received signals. As shown in eq. (2.14), the least-squares solution,  $\hat{\mathbf{o}}_{\text{LS}}$ , in eq. (2.9) becomes identical to  $\hat{\mathbf{o}}_{\text{SA}}$  when matrix **P** is orthogonal.

### 2.3 Consideration of effects of noise in estimation

To compare the effects of noise **e**, eqs. (2.9), (2.12), and (2.14) are resolved into the true components and the noise components by substituting eq. (2.6) into the respective equations.<sup>15)</sup>

The LS estimation is rewritten as

$$\begin{aligned}\hat{\mathbf{o}}_{\text{LS}} &= (\mathbf{P}^T \mathbf{P})^{-1} \mathbf{P}^T (\mathbf{P} \mathbf{o} + \mathbf{e}) \\ &= \mathbf{o} + (\mathbf{P}^T \mathbf{P})^{-1} \mathbf{P}^T \mathbf{e} \\ &= \mathbf{o} + \mathbf{V} \Sigma_{MN}^+ \mathbf{U}^T \mathbf{e}.\end{aligned}\quad (2.15)$$

If the SNR is infinite ( $\mathbf{e} = \mathbf{0}$ ), LS estimate  $\hat{\mathbf{o}}_{\text{LS}}$  is equal to the actual scattering strength distribution, **o**. However, in the case of a finite SNR, higher-order singular values are very small, particularly when the condition number,  $\sigma_1/\sigma_{MN}$ , is large. Then, the matrix 2-norm of  $\mathbf{V} \Sigma_{MN}^+ \mathbf{U}^T$  in eq. (2.15) is given by<sup>16)</sup>

$$\|\mathbf{V} \Sigma_{MN}^+ \mathbf{U}^T\|_2 = \|\Sigma_{MN}^+\|_2 = \frac{1}{\sigma_{MN}}. \quad (2.16)$$

The norm of the second term in eq. (2.15), which shows the magnitude of error, becomes enormous when  $\sigma_1/\sigma_{MN}$  is large.

Using the  $MN \times MN$  matrix  $\mathbf{I}_r = \text{diag}[1, \dots, 1, 0, \dots, 0]$ , the tSVD estimation is rewritten as

$$\begin{aligned}\hat{\mathbf{o}}_{\text{tSVD}} &= \mathbf{P}_r^+ (\mathbf{P} \mathbf{o} + \mathbf{e}) \\ &= \mathbf{V} \Sigma_r^+ \mathbf{U}^T (\mathbf{U} \Sigma \mathbf{V}^T \mathbf{o} + \mathbf{e}) \\ &= \mathbf{V} \mathbf{I}_r \mathbf{V}^T \mathbf{o} + \mathbf{V} \Sigma_r^+ \mathbf{U}^T \mathbf{e}.\end{aligned}\quad (2.17)$$

The matrix 2-norm of  $\mathbf{V} \Sigma_r^+ \mathbf{U}^T$  is  $1/\sigma_r$ . Thus, the truncation reduces the magnitude of error in eq. (2.17) to  $\sigma_r/\sigma_{MN}$  of that in eq. (2.16). For medical application, the SNR is low and the truncation order  $r$  should be set to a lower order. Then, the bias error,  $\mathbf{o} - \mathbf{V} \mathbf{I}_r \mathbf{V}^T \mathbf{o}$ , is increased due to the low-order truncation. As a result, the spatial resolution becomes low.

In the same way as above, eq. (2.14) is rewritten as

$$\begin{aligned}\hat{\mathbf{o}}_{\text{PBF}} &= \mathbf{P}^T (\mathbf{P} \mathbf{o} + \mathbf{e}) \\ &= \mathbf{V} \Sigma^T \mathbf{U}^T (\mathbf{U} \Sigma \mathbf{V}^T \mathbf{o} + \mathbf{e}) \\ &= \mathbf{V} \Lambda \mathbf{V}^T \mathbf{o} + \mathbf{V} \Sigma^T \mathbf{U}^T \mathbf{e},\end{aligned}\quad (2.18)$$

where  $\Lambda = \Sigma^T \Sigma$  is a  $MN \times MN$  matrix composed of the eigenvalues of  $\mathbf{P}^T \mathbf{P}$ . Even if the SNR is infinite, bias error is caused because matrix  $\Lambda$  is not equal to the identity matrix. However, the true scatter strength distribution **o** and noise **e** are multiplied by matrices with the 2-norm of  $\|\mathbf{V} \Lambda \mathbf{V}^T\|_2 = \sigma_1^2$  and  $\|\mathbf{V} \Sigma^T \mathbf{U}^T\|_2 = \sigma_1$ , respectively. The magnitude of the first term is more amplified than that of the second term. This means that the PBF enhances the echo signal from each point  $(x_m, z_n)$ . Thus, the PBF is effective when the SNR is low.

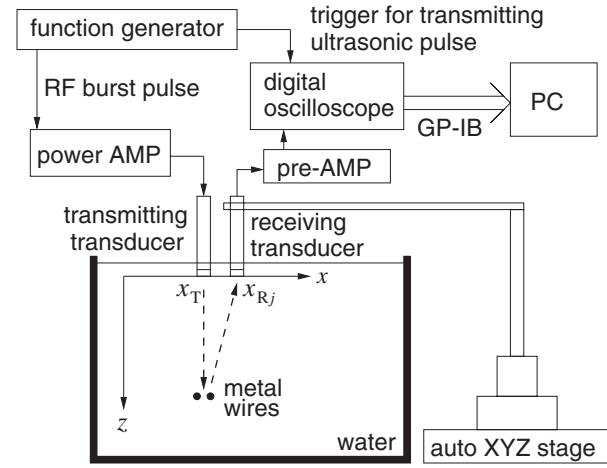


Fig. 2. Experimental setup for acquisition of simultaneously received signals using two ultrasonic transducers.

## 3. Experimental Procedure

### 3.1 Data acquisition

The experimental setup is illustrated in Fig. 2. The multichannel simultaneous reception by an array transducer is simulated with two single flat transducers (diameter  $D = 1$  mm) implementing the following data acquisition sequence. An ultrasonic pulse (center frequency  $f_c = 10$  MHz) is emitted from one of the transducers at the position  $x_T$ . The length of the Fresnel zone is  $D^2/4\lambda = 1.6$  mm. Two metal wires with a diameter of  $30 \mu\text{m}$ , which can be considered as point scatterers, are set in the water tank. The distance between two wires is 1 mm and the wires are at the same depth and symmetric with respect to the  $z$ -axis. The ultrasonic pulse is scattered by the wires and is received by the other transducer at the position  $x_{R_j}$ . The acquisition of the received signals,  $\{\mathbf{y}_j\}$ , is triggered by the transmitting pulse. The receiving transducer is moved to the next receiving point  $x_{R_{j+1}}$ , using an  $x$ -stage, for the next transmission.

### 3.2 Experimental setup

The relative positions of the simulated array and the ROI are shown in Fig. 3. Figure 4 shows the correspondence among the sampled RF data points, and their positions in the ROI. The transmitting point, the center of the simulated array, and the center of the ROI are set on the  $z$ -axis. The ROI consists of  $M \times N = 11 \times 80$  sampled points, whose intervals are  $\Delta x_m = 200 \mu\text{m}$  and  $\Delta z_n = c/(2f_s) = 14.88 \mu\text{m}$  ( $c = 1,488$  m/s at  $21.0^\circ\text{C}$ <sup>17)</sup>) along the  $x$ -axis and  $z$ -axis, respectively. The number of reception points is  $L = 61$ , and their interval is  $\Delta x_R = 200 \mu\text{m}$ . The number of samples at each receiving position is  $K = 125$  and the sampling frequency is  $f_s = 50$  MHz.

The impulse responses  $\{\mathbf{h}_j^{(m,n)}\}$  are determined from the above parameters using eqs. (2.2) and (2.3).

### 3.3 Determination of weighting function

The weighting function,  $\{w_j^{(m,n)}\}$ , in eq. (2.1) is determined from the directivity of the transducers. The directivity of flat transducer is expressed as

$$D(\theta) = \left| 2 \frac{J_1(ka \sin \theta)}{ka \sin \theta} \right|, \quad (3.1)$$

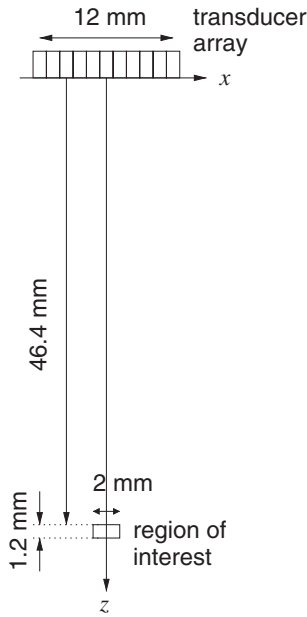


Fig. 3. Setup of the ROI and the transducer array.

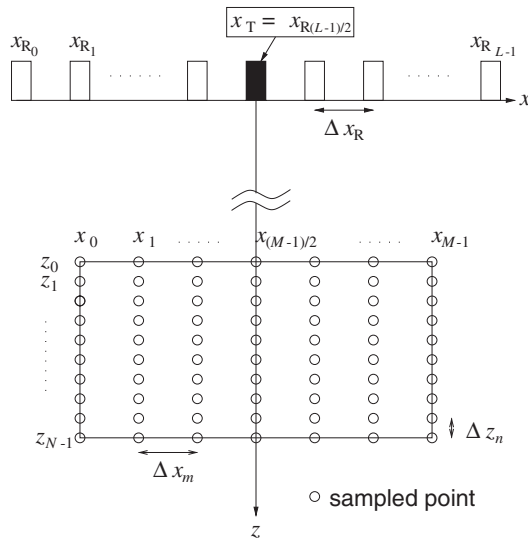


Fig. 4. Illustration of sampling of the ROI and the array.

where  $a$  is the radius of the transducer,  $k$  is the wave number, and  $J_1$  is the first-order Bessel function. Using the directivity  $D(\theta)$ , the weighting function is defined as

$$w_j^{(m,n)} = D(\theta_T) \cdot D(\theta_R), \quad (3.2)$$

where  $\theta_R$  is the receiving angle and  $\theta_T$  is the incident angle for each point  $(x_m, z_n)$ , as shown in Fig. 5. These angles are given by

$$\theta_T = \tan^{-1} \frac{x_m - x_T}{z_n}, \quad (3.3)$$

$$\theta_R = \tan^{-1} \frac{x_m - x_{R_j}}{z_n}. \quad (3.4)$$

The amplitudes of received signals are also affected by attenuation during propagation. The attenuation is caused by diffraction loss, absorption, and scattering. Since scattering does not occur in water, the attenuation factor in the weighting function is determined by diffraction and absorp-

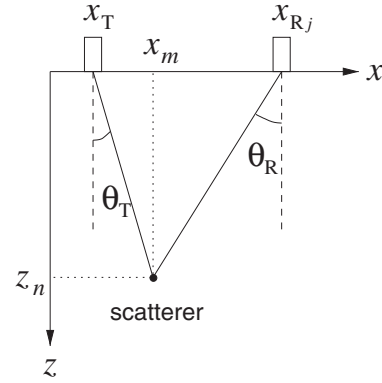


Fig. 5. Incident angle  $\theta_T$  and received angle  $\theta_R$  for point  $(x_m, z_n)$ .

tion. The amplitude of ultrasound,  $p(d)$ , after propagating through distance  $d$  is given by

$$p(d) = \frac{1}{d} p_0 e^{-\alpha d}, \quad (3.5)$$

where  $p_0$  is the amplitude at the transmitting point,  $(1/d)$  shows the diffraction loss,  $e^{-\alpha d}$  shows the absorption, and  $\alpha$  is the absorption coefficient of water. Then,  $d_j^{(m,n)}$  is the propagation distance from the transmitting point  $(x_T, 0)$  to a receiving point  $(x_{R_j}, 0)$  via a point  $(x_m, z_n)$  in the ROI, and  $d_{\min}$  is the minimum of  $d_j^{(m,n)}$ . The attenuation term of the weighting function,  $\Delta N_p$ , is determined by the ratio of  $p(d_j^{(m,n)})$  to  $p(d_{\min})$  as

$$\Delta N_p = \frac{p(d_j^{(m,n)})}{p(d_{\min})} = \left( \frac{d_{\min}}{d_j^{(m,n)}} \right) \exp[-\alpha(d_j^{(m,n)} - d_{\min})]. \quad (3.6)$$

Using  $\Delta N_p$ , the weighting function  $w_j^{(m,n)}$ , which includes the attenuation factor, is given by

$$w_j^{(m,n)} = D(\theta_T) \cdot D(\theta_R) \cdot \Delta N_p. \quad (3.7)$$

In the situation shown in Fig. 3, the influence of the attenuation term is much smaller than that of directivity ( $\min \Delta N_p = 0.97$ ) because the attenuation in water is very small and the difference between  $d_j^{(m,n)}$  and  $d_{\min}$  is small. Therefore, the weighting function is determined using eq. (3.2).

## 4. Results

### 4.1 The case of neglecting the waveform of the transmitting pulse

Here we show the estimation results when the waveform of the transmitted pulse  $s(k)$  is not considered in propagation matrix  $\mathbf{P}$  in order to compare the results obtained by tSVD with those obtained by PBF. The distribution of the singular values  $\{\sigma_i\}$  of the propagation matrix  $\mathbf{P}$  of the measurement system used in this study is shown in Fig. 6. Matrix  $\mathbf{P}$  is full rank and the unique LS solution exists because all singular values are nonzero. In this study, the truncation order  $r$  is set so that  $\sigma_r/\sigma_1$  is equal to  $-20$  dB.

The received signals,  $\{y_j\}$ , from the two wires are shown in Fig. 7. The amplitude of the received signals is represented in a gray-scale image.

The estimation results of PBF, LS, and tSVD are shown in Fig. 8. The amplitude of the estimated scattering strength is represented in color in a linear scale. To enable the

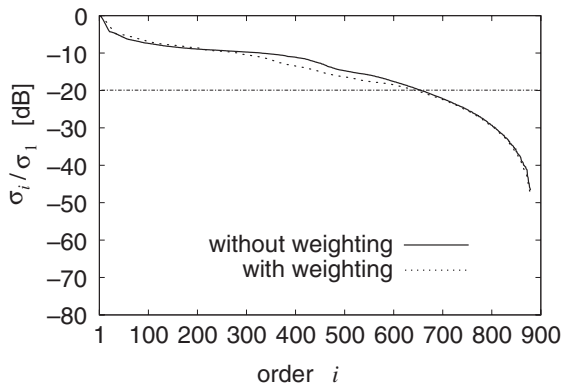


Fig. 6. Singular value distribution of propagation matrix  $\mathbf{P}$ . The transmitted pulse is not considered.

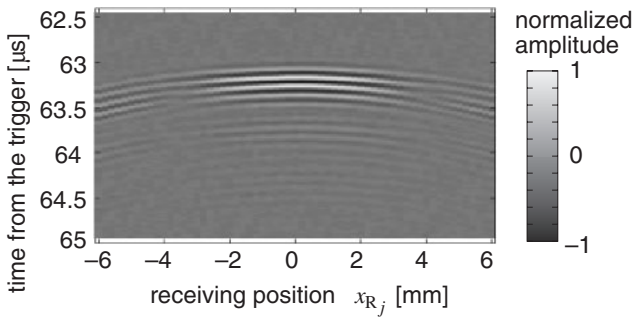


Fig. 7. Received signals  $\{y_j\}$  from two wire targets.

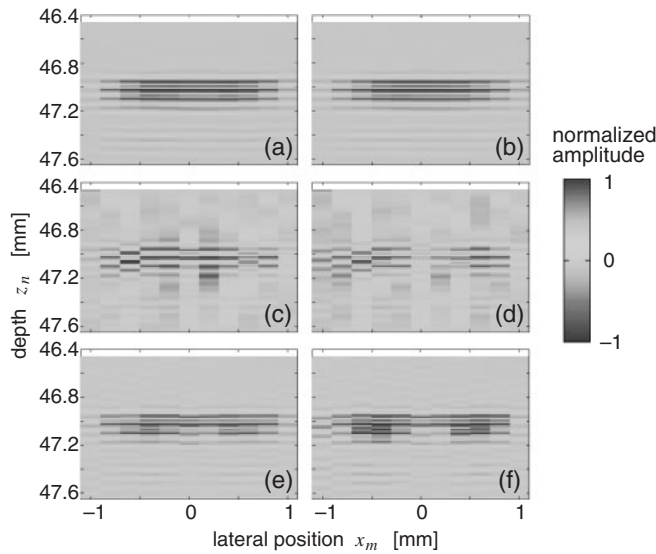


Fig. 8. Results in the case of neglecting the transmitted pulse. (a) PBF estimation  $\hat{\mathbf{O}}_{\text{PBF}}$  without weighting ( $w_{j,m} = 1$ ). (b) Weighted PBF. (c) LS estimation  $\hat{\mathbf{O}}_{\text{LS}}$  without weighting ( $w_{j,m} = 1$ ). (d) Weighted LS. (e) tSVD estimation  $\hat{\mathbf{O}}_{\text{tSVD}}$  without weighting ( $w_{j,m} = 1$ ). (f) Weighted tSVD.

comparison of different estimations, these estimation results are normalized by the maximum amplitudes of the respective estimates. The two wires are set at almost the same depths because the wavefronts in Fig. 8(a) are aligned at a certain depth. As shown in Figs. 8(c) and 8(d), the LS estimation is strongly distorted due to the influence of the smaller singular values in inverting propagation matrix  $\mathbf{P}$ . Figures 8(e) and 8(f) show that the distortion of  $\hat{\mathbf{O}}_{\text{LS}}$  is suppressed using tSVD.

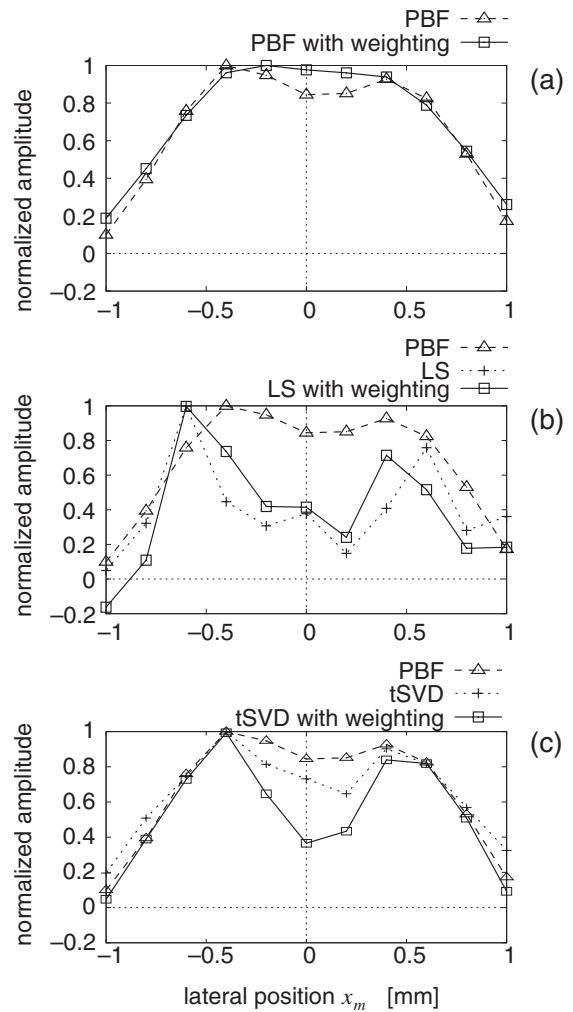


Fig. 9. Profile plots of the results shown in Fig. 8 at the depth of  $z_n = 47.06$  mm. (a) PBF estimation, (b) LS estimation, (c) tSVD estimation, with PBF estimation without weighting.

The profiles of these estimations along the  $x$ -axis at the depth of  $z_n = 47.06$  mm are shown in Fig. 9. The profile of the PBF with weighting becomes smoother than that without weighting in Fig. 9(a). On the contrary, LS and tSVD estimations do not become smooth with weighting, as shown in Figs. 9(b) and 9(c). The tSVD estimation has two significant peaks, which correspond to the positions of the wires. Furthermore, the difference between the peak values and the lowest value between peaks is larger than that in PBF, and the weighting enhances the difference. Therefore, the tSVD method is stabler than the LS method, and the performance of the tSVD with weighting is better than that of the PBF for the separation of the neighboring scatterers.

#### 4.2 The case of considering the waveform of the transmitted pulse

Now we show the estimation results when the waveform of the transmitted pulse  $s(k)$  is considered. The transmitting pulse  $s(k)$  is measured by receiving an echo from a glass plate. The measured waveform is shown in Fig. 10. The singular value distribution of matrix  $\mathbf{P}$ , in which  $s(k)$  is considered, is shown in Fig. 11. Compared with Fig. 6, the higher-order singular values become very small because  $s(k)$  is a narrow band signal in comparison with the impulse

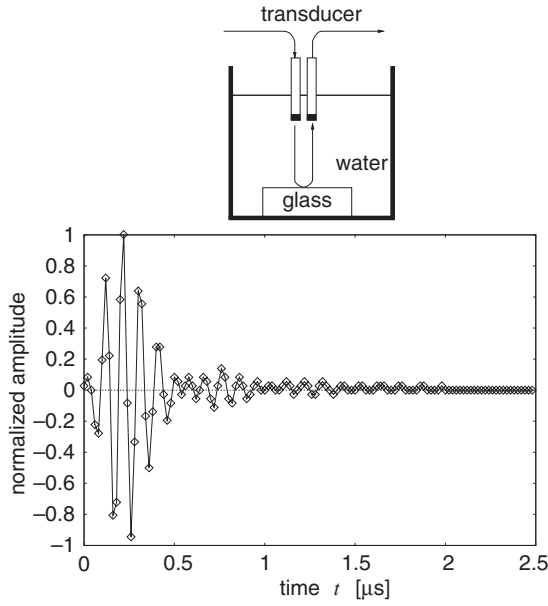


Fig. 10. Waveform of transmitted pulse  $s(k)$ .

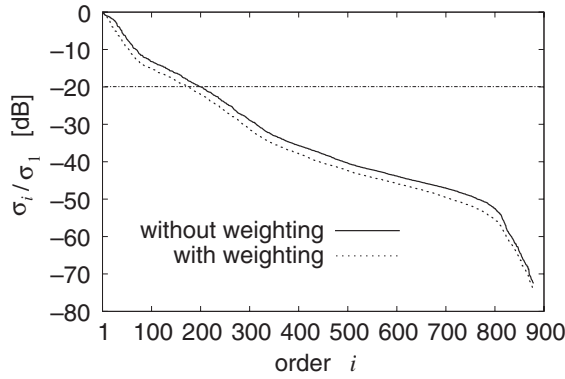


Fig. 11. Singular value distribution of propagation matrix  $\mathbf{P}$ . The transmitted pulse is considered.

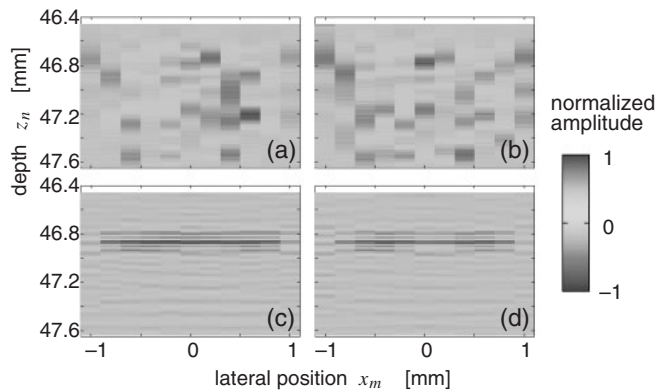


Fig. 12. Results in the case of considering transmitted pulse. (a) LS estimation  $\hat{\mathbf{O}}_{LS}$  without weighting ( $w_{j,m} = 1$ ). (b) Weighted LS. (c) tSVD estimation  $\hat{\mathbf{O}}_{tSVD}$  without weighting ( $w_{j,m} = 1$ ). (d) Weighted tSVD.

assumed in §4.1. As in §4.1, the truncation order  $r$  is set to be a value of the order at  $\sigma_r/\sigma_1 = -20$  dB.

The estimation results of LS and tSVD are shown in Fig. 12. The distortions of LS estimations shown in Figs. 12(a) and 12(b) are stronger than those in Figs. 8(c)

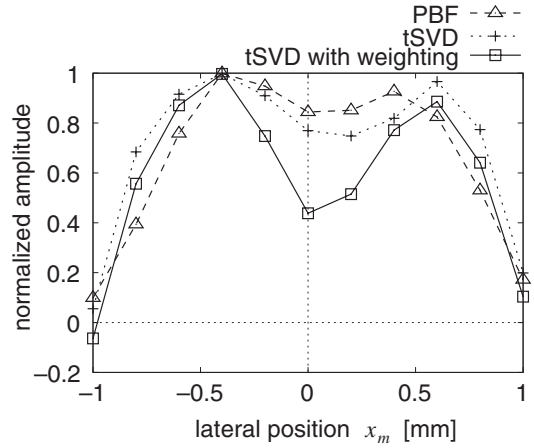


Fig. 13. Profile plots of the results shown in Figs. 12(c) and 12(d) at the depth of  $z_n = 46.89$  mm.

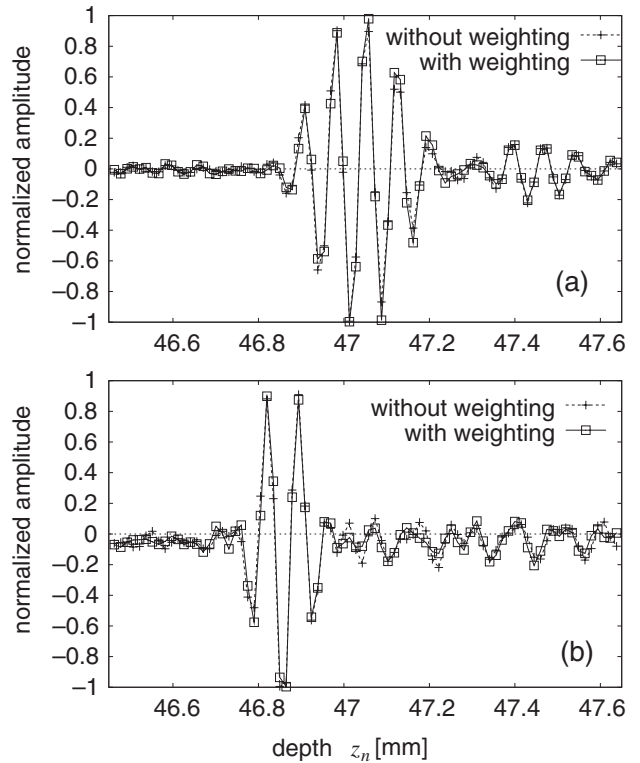


Fig. 14. Profile plots of the tSVD estimation along  $z$ -axis at  $x_m = -0.4$  mm. (a) Results in the case of neglecting the transmitted pulse shown in Figs. 8(e) and 8(f). (b) Results in the case of considering the transmitted pulse shown in Figs. 12(c) and 12(d).

and 8(d). As shown in Figs. 12(c) and 12(d), the strong noise amplification is suppressed using tSVD. The profiles of estimations of tSVD along the  $x$ -axis at the depth of  $z_n = 46.89$  mm are shown in Fig. 13 compared with the PBF profile shown in Fig. 9(a). Using tSVD and weighting, a higher lateral resolution was achieved.

The profiles along the  $z$ -axis at  $x_m = -0.4$  mm of Figs. 8(e), 8(f), 12(c), and 12(d) are shown in Figs. 14(a) and 14(b), respectively. The transmitted pulse component is directly appears in Fig. 14(a). On the other hand, the pulse duration becomes short when considering  $s(k)$  in matrix  $\mathbf{P}$ , as shown in Fig. 14(b) [the estimate became close to an impulse (= scattering strength)].

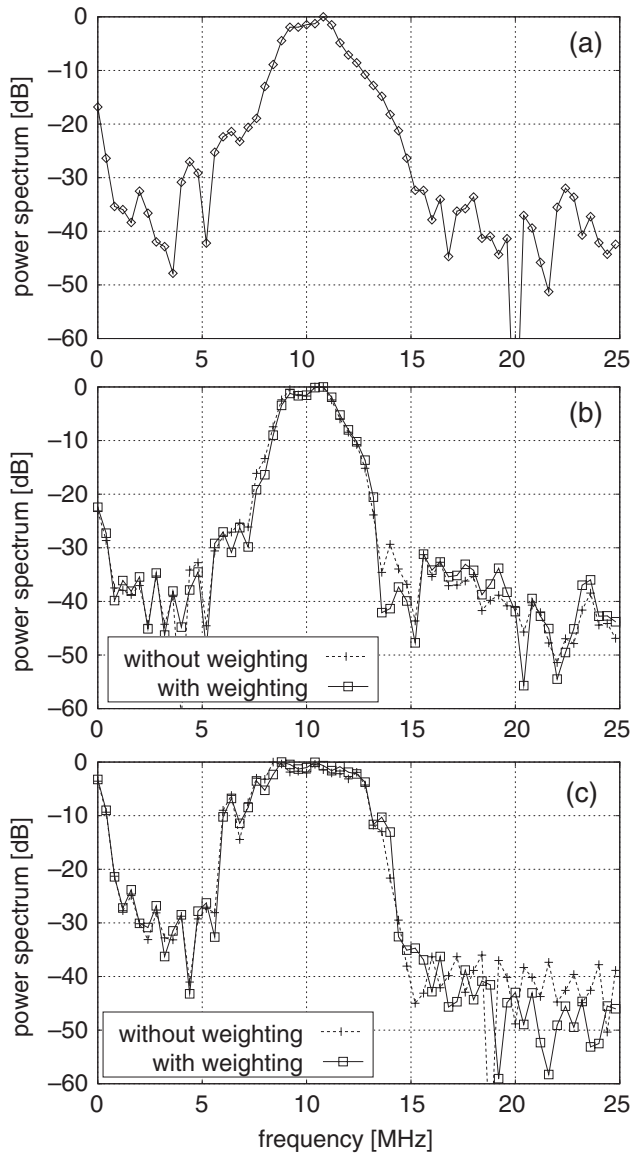


Fig. 15. (a) Power spectrum of the transmitted pulse  $s(k)$ . (b) Power spectra of the profiles shown in Fig. 14(a). (c) Power spectra of the profiles shown in Fig. 14(b).

The power spectra of these profiles along the  $z$ -axis are shown in Fig. 15. Figure 15(a) shows the power spectrum of the transmitted pulse  $s(k)$ . The bandwidth of the estimate without considering  $s(k)$  shown in Fig. 15(b) is similar to that of in Fig. 15(a). As shown in Fig. 15(c), the bandwidth of the estimate considering  $s(k)$  is broadened around the

center frequency of 10 MHz, which corresponds to the improvement in the axial resolution by the convolution of the transmitted pulse and the impulse response.

### 5. Conclusions

In this study, we constructed an experimental setup for the simulation of multichannel simultaneous reception of echo signals by a linear array transducer using two single-element ultrasonic transducers. The echo signals from two fine wires were acquired, and the scattering strength distribution in the ROI was estimated. Compared with the PBF, the tSVD method with weighting was effective in separating the neighboring scatterers. The results showed a potential of the proposed method for B-mode imaging with a high spatial resolution at a high frame rate. It is considered that the tSVD method is effective for NDE applications. In medical applications, the SNR is low and a lower-order truncation, which leads to a degradation of spatial resolution, is necessary.

- 1) S. I. Nikolov and J. A. Jensen: *IEEE Trans. Ultrason. Ferroelectr. Freq. Control* **50** (2003) 848.
- 2) Y. Minochi, S. Yagi, and T. Nishiyama: *Jpn. J. Appl. Phys.* **43** (2004) 3103.
- 3) M. Tanter, J. Bercoff, L. Sandrin, and M. Fink: *IEEE Trans. Ultrason. Ferroelectr. Freq. Control* **49** (2002) 1363.
- 4) G. R. Lockwood, J. R. Talman, and S. S. Brunke: *IEEE Trans. Ultrason. Ferroelectr. Freq. Control* **45** (1998) 980.
- 5) S. Ishigami, H. Yanagida, Y. Tamura, C. Ishihara, and N. Okada: *Jpn. J. Appl. Phys.* **42** (2003) 3276.
- 6) O. T. von Ramm, S. W. Smith, and H. G. Pavy, Jr.: *IEEE Trans. Ultrason. Ferroelectr. Freq. Control* **38** (1991) 109.
- 7) M. Karaman, P. C. Li, and M. O'Donnell: *IEEE Trans. Ultrason. Ferroelectr. Freq. Control* **42** (1995) 429.
- 8) M. Tanter, J. L. Thomas, and M. Fink: *J. Acoust. Soc. Am.* **108** (2000) 223.
- 9) F. Lingvall: *Ultrasonics* **42** (2004) 961.
- 10) E. Wennerström, T. Stepinski, and T. Olofsson: *IEEE Trans. Ultrason. Ferroelectr. Freq. Control* **53** (2006) 1008.
- 11) H. Desoky, A. B. M. Youssef, and Y. M. Kadah: *Proc. SPIE* **5035** (2003) 147.
- 12) F. Lingvall, T. Olofsson, and T. Stepinski: *J. Acoust. Soc. Am.* **114** (2003) 225.
- 13) A. Ishimaru: *Wave Propagation and Scattering in Random Media* (IEEE Press, Piscataway, 1999) p. 494.
- 14) F. Lingvall: Ph. D. dissertation, Uppsala University, Uppsala, Sweden, 2004.
- 15) H. Kanai and K. Kido: *IEEE Trans. Signal Process.* **39** (1991) 148.
- 16) G. H. Golub and C. F. Van Loan: *Matrix Computations* (Johns Hopkins University Press, Baltimore, 1989) 2nd ed., p. 70.
- 17) G. W. Willard: *J. Acoust. Soc. Am.* **19** (1947) 235.